Development of the prototype for the SPARC hard X-ray monitor

E. Panontin ✉ (ORCID) ; R. A. Tinguely (ORCID) ; Z. S. Hartwig (ORCID) ; A. A. Saltos; D. Vezinet (ORCID) ; J. Rice (ORCID)

Check for updates

View Online   Export Citation

Development of the prototype for the SPARC hard X-ray monitor

View Online   Export Citation   CrossMark

E. Panontin,[1,a] ⬤ R. A. Tinguely,[1] ⬤ Z. S. Hartwig,[1] ⬤ A. A. Saltos,[2] D. Vezinet,[2] ⬤ and J. Rice[1] ⬤

AFFILIATIONS

[1] Plasma Science and Fusion Center, MIT, Cambridge, Massachusetts 02139, USA
[2] Commonwealth Fusion Systems, Devens, Massachusetts 01434, USA

Note: This paper is part of the Special Topic on Proceedings of the 25th Topical Conference on High-Temperature Plasma Diagnostics.
[a] Author to whom correspondence should be addressed: panontin@psfc.mit.edu

ABSTRACT

The SPARC tokamak will be equipped with a hard X-ray (HXR) monitor system capable of measuring the bremsstrahlung emission from runaway electrons with photon energies in excess of about 100 keV. This diagnostic will detect the formation of runaway electron beams during plasma start-up and inform the plasma control system to terminate the discharge early to protect the machine. In this work, we present a 0D estimate of the HXR emission in SPARC during plasma start-up. Then we discuss the characterization of a prototype of the HXR monitor. The detector mounts a 1×1-in.^{2} LaBr$_3$ inorganic scintillator coupled with a photomultiplier tube and has been tested with γ-ray sources to find its dynamic range. Finally, two possible modes of operation for spectroscopic and current mode measurements on SPARC are proposed.

I. INTRODUCTION

Start-up runaway electrons (REs) are relativistic particles that can be generated during plasma start-up in tokamaks when a high toroidal electric field is applied to a low density gas to cause plasma break-down and then increase plasma current. In most cases, REs drive a modest current and are harmlessly dissipated or lost at a constant rate on the plasma facing components (PFCs).[1] In other discharges, start-up REs can end up driving a significant fraction of the plasma current.[1] When that happens, REs reach high energies at which they lose magnetic confinement, and their impact on the PFCs might cause severe damage.[1–3]

The SPARC tokamak[4] will be equipped with a set of diagnostics[5,6] that will monitor the formation of start-up RE beams. These diagnostics will stream data to the plasma control system (PCS) (a system that monitors the plasma thanks to real-time data flows from multiple diagnostics and implements feedback control loops on actuators) in real time to inform an early shutdown of the discharge if start-up REs are detected. Among these diagnostics, the hard X-ray (HXR) monitors[6] will observe MeV-range photons

emitted by runaway electrons undergoing bremsstrahlung scattering on plasma ions and on the machine PFCs.

The experience developed on other machines, such as JET, C-MOD, and KSTAR, suggests that the HXR signal during plasma start-up mostly comes from constant RE losses on outer limiters[1,3] and can be anisotropic.[3] SPARC will have a continuous toroidal inner limiter and 18 outer limiters. Tolerances in their installation might favor the dissipation of start-up REs in certain localized regions. The uniformity of the RE collisions with PFC is hard to predict and will be studied experimentally during early campaigns. In the scope of this paper, we will assume the RE losses to be uniform, and in Sec. II, we will estimate the HXR emission spectrum in SPARC using a 0D model[7–9] coupled with the MCNP code[10] for photon transport.

In Sec. III, we will discuss the preliminary design of SPARC HXR monitors, which considers two LaBr$_3$ inorganic scintillators that will measure photon energies in excess of 100 keV, and a CdTe based detector located in the diagnostics hall on a collimated line of sight that will measure photon energies between 10 and 200 keV. To ensure early detection of start-up RE beams, the LaBr$_3$ detectors

will be placed in the torus hall and will have a wide field of view (FOV) that covers the entire poloidal section of the tokamak. Their toroidal FOV should maximize the portion of limiters observed by the diagnostics and allow measurements in both plasma current directions.

Finally, Sec. IV describes the state of the prototype for the HXR monitors that are currently being tested at MIT. The hardware selection has been guided by the work carried out on other machines. Alcator C-Mod experience with a monitor for start-up REs based on a BGO crystal digitized at 1 MSps[11] was considered for developing a current mode duty cycle for our prototype. ASDEX Upgrade experience with a LaBr$_3$ crystals[12] for post-disruption runaway studies has been considered for hardware selection and for implementing a spectroscopy duty cycle. For SPARC, the prototype mounts a 1×1-in.^{2} LaBr$_3$ inorganic scintillator coupled with a photomultiplier tube (PMT), but other crystals, such as BGO, will also be tested in the future. The detector characterization in terms of energy resolution, time response, and dynamic range is discussed. Different options for current mode and spectroscopic data acquisitions are also compared, presenting possible digitization schemes for recording both signals at the same time.

II. HXR SIGNAL

The HXR emission from REs has been estimated following the 0D approach developed in Refs. 7–9:

$$
\begin{aligned}
dR_B = n_I (&n_{RE} \, f_{RE} \, v_{RE} \, dE_{RE}) \\
&\times \frac{d^2\sigma}{dE_{HXR} \, d\Omega} (E_{RE}, E_{HXR}, \cos(\theta)) \\
&\times dE_{HXR} \, d\Omega \, dV,
\end{aligned}
\tag{1}
$$

where R_B is the bremsstrahlung reaction rate (p/s). $\frac{d^2\sigma}{dE_{HXR} \, d\Omega}$ is the semi-analytical bremsstrahlung double differential cross section (m^{-2} J^{-1}) derived in Refs. 13 and 14. It is a function of the RE energy E_{RE} (J), the HXR energy E_{HXR} (J), and θ (rad) the angle of emission of the HXR with respect to the RE velocity. $d\Omega$ (srad) is the solid angle subtended by the detector and dV (m^3) is the plasma volume where the emission takes place. n_I (m^{-3}) is the ion density and n_{RE} (m^{-3}) is the RE density. Finally, v_{RE} (m/s) is the RE velocity and f_{RE} (J^{-1}) is the RE distribution function.

The HXR emission has been divided into two categories: those coming from RE interactions with plasma ions (thin-target) and those coming from RE collisions with PFCs (thick target). For thin-target, n_I is 10^{20} m^{-3}, while n_{RE} has been set assuming a current carried by REs of $I_{RE} = 1$ kA and a beam located around SPARC major radius $R_0 = 1.85$ m. f_{RE} is considered exponentially decreasing, and the maximum energy of the RE beam shown in Fig. 2 is defined as the 99.9 percentile of f_{RE}. $d\Omega$ has been estimated assuming a 1×1-in.^{2} (diameter × height) cylindrical detector installed close to the Diagnostic Hall Wall, at 13 m from the plasma. For thick-target, we assume that most of the REs will impact the tungsten of the outer limiter[1] with a velocity tangential to the limiter surface. n_I is 6×10^{28} m^{-3} and n_{RE} has been calculated according to Ref. 1, Eq. 5, with confinement time $\tau_{RE} = 1.7$ s extrapolated from Ref. 1, Fig. 9. Since the cross-section is peaked toward forward emission,[7,15] we can set $\theta = 0$ and assume most of the HXR signal will come from
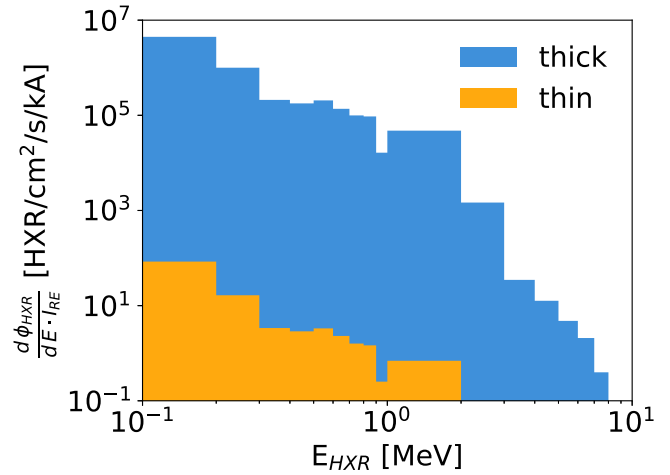

FIG. 1. Spectrum of the HXR flux ($\frac{d\phi_{HXR}}{dE \cdot I_{RE}}$) at the HXR monitor position from an exponential RE distribution with 10 MeV maximum energy and normalized by the RE current in kA. Signals due to interactions with plasma ions (thin target) and losses on PFCs (thick target) are compared.

the limiter having a surface parallel to the detector LOS. The emitted HXR spectrum has then been propagated to the HXR monitors' position using MCNP simulations, which are summarized in Figs. 1 and 2. Figure 1 shows the spectrum of the HXR flux at the detector position for both thin and thick target emissions: using the loss rates reported in Ref. 1, thick-target dominates the HXR signal. Figure 2 shows the total flux impinging on the detector as the RE maximum energy ranges between 0.1 and 10 MeV, which are the typical energies observed on other machines during plasma start-up.[1]
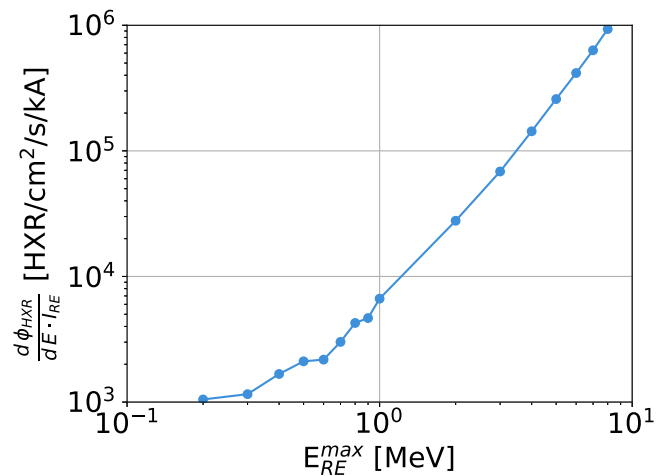

FIG. 2. Total HXR flux ($\frac{d\phi_{HXR}}{dE \cdot I_{RE}}$) at the HXR monitor position as a function of RE maximum energy and normalized by the RE current in kA.

III. THE HXR MONITOR PROTOTYPE

The prototype of the HXR monitor for SPARC is based on two precedents installed at Alcator C-Mod[11] and ASDEX Upgrade[12] tokamaks and aims at performing current mode measurements while scoping opportunities for simultaneous spectroscopic operations. An overview of the detector and digitization chain is shown in Fig. 3. The detector mounts a 1×1-in.^{2} LaBr$_3$ inorganic scintillator[16] coupled with a H10828 PMT from Hamamatsu,[17] which can operate between $[-1500, -500]$ V and can sustain a maximum average anode current of 0.39 mA. The scintillator and PMT are enclosed in a custom-made light-tight aluminum case.

The PMT anode signal is connected to the digitizer with a 90 cm long BNC to MCX cable. On SPARC, we expect the cable carrying the signal to be of the order of 10 m long, which will affect the noise and resolution of the measurements. The digitizer used for these tests is a first generation DT5730s digitizer[18] (500 MSps, 14 bits, 2 V$_{pp}$) from CAEN that communicates with a PC via a universal serial bus (USB) (30 MB/s bandwidth). The digitizer runs the Digital Pulse Processing for Charge Integration and Pulse Shape Discrimination (DPP-PSD) firmware, which is capable of storing the waveforms of single events and performing a real time digital integration of the charge associated with each event. The charge coarse gain for the digitization process, that is, the minimum charge increase necessary to increase by 1 least significant bit (LSB) the energy of the pulse, can be set by the user depending on the dynamic range of interest.

The detector can be operated in two modes—current or spectroscopic mode—with two dedicated duty cycles. In the current mode, an external pulse generator is used to trigger the digitizer at 10 kHz, which is the frequency at which the PCS will read the HXR current during SPARC operations. The digitizer then stores locally a segment of data 100 μs long and transfers to the computer only the integrated charge. Transferring the whole waveform in real-time would require a bandwidth of 1 GB/s, which is beyond the capabilities of any digitizer of which we know. Also, the internal memory of our digitizer would not be able to store the waveforms for the entire duration of a SPARC start-up phase. Thus, in spectroscopic mode, the acquisition self triggers when the detector signal exceeds a certain threshold and a segment of data (with a record length typically around 200 ns) is stored. If the whole waveform is saved on the computer, then the digitizer–computer communication saturates at about 100 kCps.

IV. PROTOTYPE CHARACTERIZATION

The prototype of the HXR monitor for SPARC, described in Sec. III, has been characterized by means of ^{137}Cs and ^{22}Na gamma sources that emit three characteristic γ-rays of ^{137}Cs (662 keV) and ^{22}Na (511 and 1275 keV). In this section, we discuss the energy calibration of the detector, which is then used to estimate its dynamic range in both spectroscopic and current modes. The waveform of a single photon interaction is also analyzed to estimate the maximum event rate sustainable by the detector. For all these tests, the PMT has been operated at a low voltage bias of -600 V, which ensures a larger dynamic range for spectroscopic measurements when compared with a higher absolute PMT voltage bias. We envision using the same bias for current mode experiments on SPARC. The digital acquisition (DAQ) energy gain was set to 80 fC/LSB (i.e., for every 80 fC deposited in the detector, the DAQ energy of the photon is increased by one).

A. Energy calibration

The spectrum of the ^{137}Cs and ^{22}Na sources measured with the LaBr$_3$ detector is shown in Fig. 4 over the environmental background: the three photo-peaks with their Compton shoulders are clearly visible. A fitting routine has been employed to find the peak position and width, from which the calibration of the DAQ channel axis and the detector resolution have been calculated. The resolution of the detector at the ^{137}Cs peak is 4.3%, which is in line with other LaBr$_3$ detectors.[8,12,19,20]

The background of the measurement is composed of the intrinsic emission of the crystal and the radiation coming from the laboratory environment. The α-decay of ^{227}Ac impurities in the crystal can be identified above 1.6 MeV, as reported by the manufacturer.[16] Between 1.4 and 1.5 MeV, there is a characteristic γ-peak due to the superposition of a 1.473 MeV peak from ^{138}La and a 1.441 MeV peak from the ^{40}K contained in the crystal[16] and the environment.

FIG. 3. Prototype of the SPARC HXR monitor: LaBr$_3$ crystal + PMT enclosed in an aluminum case, CAEN DT5730s digitizer, CAEN DT1471ET high-voltage module, and Agilent 33220A pulse generator.
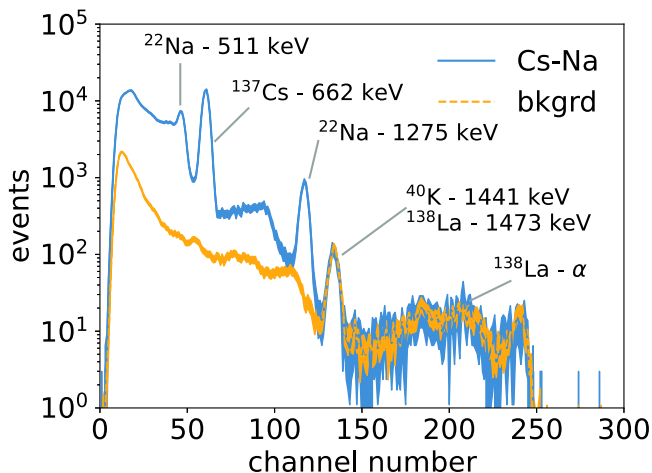
FIG. 4. Calibration spectrum (blue solid line) measured with the LaBr$_3$ detector. The calibration peaks of the ^{137}Cs (662 keV) and ^{22}Na (511, 1275 keV) gamma sources are highlighted. The ^{138}La γ-peak (1473 keV), ^{40}K γ-peak (1441 keV), and ^{227}Ac alpha decays are also visible in the measurement background (yellow dashed line). The width of the curves represents two Poissonian standard deviations of the measured counts. The horizontal axis reports the energy deposited in the detector by a single photon, calculated as the area of the pulse and expressed in DAQ channels.

At lower energies, the 789 keV γ-decay of ^{138}La overlaps with the β-decay of the same element and with the background coming from the laboratory, leading to a continuum spectrum.

The calibration of the DAQ channels is shown in Fig. 5 together with the dynamic range of the LaBr$_3$ detector. At the energies of the ^{137}Cs and ^{22}Na sources, the PMT response to γ-ray energy has
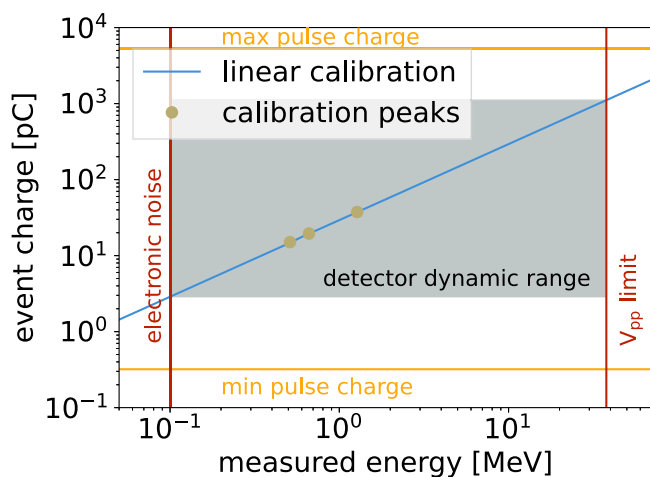

FIG. 5. Linear energy calibration of the LaBr$_3$ detector (blue line). DAQ channels are expressed in units of integrated charge (pC). The positions of the peak in Fig. 4 are shown in dots, and their errors are within the marker size. The red vertical lines show the dynamic range for the voltage digitization, while the yellow horizontal lines show the dynamic range for the integrated charge digitization.

been described with a linear model. The calibration is then linearly extrapolated to higher energies for studying the dynamic range of the detector.

B. Spectroscopic dynamic range

For spectroscopic measurements, the energy dynamic range is determined by the digitization of the input voltage. The voltage range of the digitizer is 2 V$_{pp}$, with 14 bits resolution (16384 DAQ channels). Based on the detector calibration, the maximum measurable photon energy is 35 MeV. At low energy, the dynamic range is limited by the electronic noise in the digitization chain, which at −600 V was measured to extend up to about 100 keV. In order to filter out this noise, a low energy threshold is set so that the digitizer ignores any signal below 100 keV. The acquisition settings and dynamic range for spectroscopy are reported in Table I. Figure 5 shows the energy-charge conversion for single pulses and the dynamic range of the detector.

C. Current mode dynamic range

For current mode measurements on SPARC, the digitizer will integrate the voltage signal over 0.1 ms. The dynamic range is determined by the waveform charge digitization, which is performed on a 16 bit register that is then bit-shifted to a 14-bit data format. The other limiting factor is the maximum average anode current the PMT can sustain, which for our model is about 0.39 mA, or 39 nC integrated over 0.1 ms.

Figure 1 can be convolved with Fig. 5 to estimate the current flowing through the PMT anode for the expected HXR spectrum on SPARC. On SPARC, the optimal digitizer coarse gain is estimated to be 1280 fC/LSB for a PMT bias of −600 V. The detector saturates at event rates of 10^8–10^9 counts per second (Cps) depending on the maximum RE energy. If we assume an exponential RE distribution with 10 MeV maximum energy, the detector would saturate at an I_{RE} of about 100 kA. This maximum current can be tuned by changing the PMT voltage, crystal size, or material if a wider dynamic range is needed. With these gain settings, the minimum charge that can be measured would correspond to a single HXR that deposits 0.2 MeV energy in the crystal, which is similar to the low energy cut used for filtering out electronic noise. A summary of the acquisition settings and dynamic range for the current mode is reported in Table I.

D. Detector waveform

The time trace of the anode voltage $V(t)$, also called the waveform, following the interaction of a single photon depositing an energy of 662 keV in the detector is reported in Fig. 6. The voltage

TABLE I. Digitizer settings for spectroscopic and current mode measurements on SPARC. The diagnostic dynamic range in energy and maximum count rate are also reported for each operation mode.

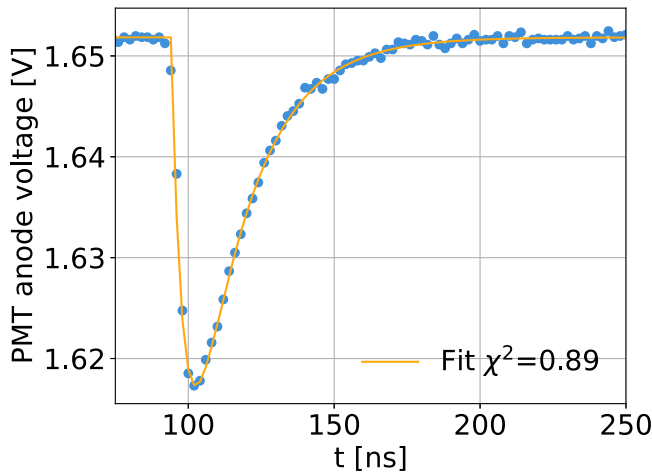|	Gain (fC/LSB)	Integration time (ns)	Dynamic range (MeV)	Max rate (Cps)
Spectroscopy	80	130	(0.1, 30)	10^6
Current	1280	0.1	>0.2	10^8

FIG. 6. Example of a waveform for a 662 keV event (blue dots). The result of data fitting with Eq. (3) is shown with a yellow line.

(V) can be converted into the charge (C) deposited in the detector according to

$$dQ(t) = \frac{V(t)\,dt}{R},\qquad(2)$$

where $R = 50\ \Omega$ is the input resistance of the digitizer and $dt = 2$ ns is the sampling rate of the digitizer. This formula has been used to calculate the energy of the pulse from the waveform. $V(t)$ has been fitted with an analytic formula describing the rise and decay time of the crystal,[19]

$$V(t) = \begin{cases} V_0 & \text{if } t < t_0 \\ V_0 - \dfrac{A}{t_d - t_r}\left[e^{-\frac{t-t_0}{t_r}} - e^{-\frac{t-t_0}{t_d}}\right] & \text{if } t > t_0 \end{cases},\qquad(3)$$

where V_0 (V) is the baseline of the waveform calculated from the samples measured before the trigger, A (V s) is the integral of the waveform, t_0 (s) is the initial time at which the photon entered the detector, t_r (s) is the rise time of the signal, and t_d (s) is the primary decay time of the crystal. The fit converges: the goodness of fit test yields a reduced-$\chi^2 = 0.89$ and p-value $= 0.9$ (p-value threshold of significance is set to 0.05 as usual). The fit's result is included in Fig. 6: the crystal has a $t_r = 4.5$ ns and $t_d = 18.6$ ns, which are consistent with what is reported by the producer.[16]

Figure 6 also shows the width of the pulse, $\Delta t \approx 100$ ns, which is calculated as the width of the peak at 1% of the peak. If only 100 ns of the waveform were recorded, the error in the reconstruction of the energy of the pulse would be around 0.7%. Considering this pulse width and a pre-trigger time of 32 ns for baseline evaluation, we can estimate the minimum record length necessary to perform spectroscopy on SPARC using a fast crystal like LaBr$_3$ to be $\Delta t_{RL} \approx 130$ ns. Minimizing the record length for the spectroscopic mode of acquisition minimizes the pile-up levels at high rates. A

model based on Poissonian statistics and a non-paralyzed detector has been used for estimating the expected pile-up levels at various rates for a record length of 130 ns. Previous works on MeV-range photon spectroscopy and pile-up restoration show that spectroscopy can be performed up to a count rate of about 1 MCps,[19–21] at which the pile-up level would be about 25%. Thus, a pileup restoration routine should be adopted in preparation for SPARC operations. Shortening the record length also reduces the requirements in terms of bandwidth communication between the digitizer and the computer of the acquisition, which can be calculated as the product of the record length, the acquisition sampling rate (500 MSps), the bytes stored per sample, and the count rate at the detector (up to 1 MCps). To stream 130 ns waveforms, a bandwidth greater than $\Delta t_{RL} \cdot 500$ MSps $\cdot 2$ Bytes $\cdot 1$MCps $= 130$ MB/s is needed for each active channel, which exceeds the capabilities of the digitizer used for the tests reported in this work (see Sec. III).

V. CONCLUSIONS

A 0D estimate of the HXR signal levels in the SPARC torus hall close to the diagnostics hall wall has been presented. The comparison of the contributions of thin and thick-target emissions suggests that the HXR measurements during SPARC plasma start-up will be dominated by collisions of REs with the limiters. This result is based on a scaling law for the start-up RE confinement time and should be verified using orbit tracing codes to estimate the RE loss rate and impact positions. An estimate of the HXR spectrum and total flux impinging on the detector is also given. The assembly of the prototype for the SPARC HXR monitor and its characterization with lab tests are also presented. The detector is made of a 1 × 1 in.^{2} LaBr$_3$ crystal with demountable PMT and is enclosed in a custom-made, light-tight Al case. Two routines have been implemented to operate the detector in current mode and spectroscopic mode. The detector characterization shows performance in line with previous detectors for energy resolution and crystal decay times. From the detector calibration, two different operation states have been identified for spectroscopic and current modes. Their dynamic ranges have been calculated, showing that the current prototype would saturate at about 10^8–10^9 Cps in the current mode. Limitations in the data transfer rate with the present prototype have been encountered. Alternative digitizers with faster computer–digitizer communication or internal memory will be tested to enable the HXR monitor to store the full waveforms over a whole SPARC discharge.

AUTHOR DECLARATIONS

Conflict of Interest

The authors have no conflicts to disclose.

10 September 2024 17:06:29

Author Contributions

E. Panontin: Conceptualization (equal); Data curation (lead); Formal analysis (lead); Investigation (lead); Methodology (lead); Software (lead); Visualization (lead); Writing – original draft (lead); Writing – review & editing (lead). **R.A. Tinguely**: Conceptualization (equal); Formal analysis (equal); Funding acquisition (supporting); Investigation (equal); Methodology (supporting); Resources (equal); Supervision (lead); Visualization (equal); Writing – review & editing (equal). **Z.S. Hartwig**: Resources (equal); Software (equal); Supervision (supporting); Writing – review & editing (supporting). **A. A. Saltos**: Data curation (supporting); Formal analysis (equal); Software (supporting); Visualization (supporting). **D. Vezinet**: Conceptualization (equal); Funding acquisition (supporting); Investigation (supporting); Methodology (supporting); Supervision (equal); Writing – review & editing (equal). **J. Rice**: Conceptualization (supporting); Funding acquisition (lead); Investigation (supporting); Resources (supporting); Supervision (supporting); Writing – review & editing (supporting).

DATA AVAILABILITY

The data that support the findings of this study are available from the corresponding author upon reasonable request.

REFERENCES

[1] P. de Vries, Y. Lee, Y. Gribov, A. Mineev, Y. Na, R. Granetz, B. Stein-Lubrano, C. Reux, P. Moreau, V. Kiptily *et al.*, Nucl. Fusion **63**, 086016 (2023).

[2] R. Granetz and B. Stein-Lubrano, "Study of Alcator C-Mod discharges that had startup runaways," in 34th ITPA MHD, 2020.

[3] J. Rice, "The electron distribution function and impurities in Alcator," Ph.D. thesis, MIT, 1979.

[4] A. Creely, M. Greenwald, S. Ballinger, D. Brunner, J. Canik, J. Doody, T. Fülöp, D. Garnier, R. Granetz, T. Gray *et al.*, J. Plasma Phys. **86**, 865860502 (2020).

[5] M. Reinke, I. Abramovic, A. Albert, K. Asai, J. Ball, J. Batko, J. Brettingen, D. Brunner, M. Cario, J. Carmichael *et al.*, "Overview of the early campaign diagnostics for the SPARC tokamak," Rev. Sci. Instrum. (submitted) (2024), these proceedings.

[6] D. Vezinet, C. J. Perks, E. Panontin, S. Normile, R. A. Tinguely, J. Rice, M. Reinke, M. Cario, J. Raimond, A. Hoffmann *et al.*, "SPARC x-ray diagnostics: Technical and functional overview," Rev. Sci. Instrum. (submitted) (2024), these proceedings.

[7] S. P. Pandya, L. Core, R. Barnsley, J. Rosato, R. Reichle, M. Lehnen, L. Bertalot, and M. Walsh, Phys. Scr. **93**, 115601 (2018).

[8] M. Nocente, M. Tardocchi, R. Barnsley, L. Bertalot, B. Brichard, G. Croci, G. Brolatti, L. D. Pace, A. Fernandes, L. Giacomelli *et al.*, Nucl. Fusion **57**, 076016 (2017).

[9] E. Panontin, A. D. Molin, M. Nocente, G. Croci, J. Eriksson, L. Giacomelli, G. Gorini, M. Iliasova, E. Khilkevitch, A. Muraro *et al.*, J. Instrum. **16**, C12005 (2021).

[10] C. J. Werner, J. S. Bull, C. J. Solomon, F. B. Brown, G. W. McKinney, M. E. Rising, D. A. Dixon, R. L. Martz, H. G. Hughes, L. J. Cox *et al.*, "MCNP version 6.2 release notes," Technical Report No. LA-UR-18-20808, Los Alamos National Laboratory (LANL), 2018.

[11] E. Marmar, A. Bader, M. Bakhtiari, H. Barnard, W. Beck, I. Bespamyatnov, A. Binus, P. Bonoli, B. Bose, M. Bitter *et al.*, Nucl. Fusion **49**, 104014 (2009).

[12] A. D. Molin, M. Nocente, M. D. Rosa, E. Panontin, D. Rigamonti, M. Tardocchi, A. Shevelev, E. Khilkevitch, M. Iliasova, L. Giacomelli *et al.*, Meas. Sci. Technol. **34**, 085501 (2023).

[13] F. Salvat and J. Fernández-Varea, Nucl. Instrum. Methods Phys. Res., Sect. B **63**, 255–269 (1992).

[14] F. Salvat, J. Fernández-Varea, J. Sempau, and X. Llovet, Radiat. Phys. Chem. **75**, 1201–1219 (2006).

[15] E. Panontin, M. Nocente, A. D. Molin, J. Eriksson, G. Gorini, E. P. Cippo, D. Rigamonti, M. Salewski, and M. Tardocchi *et al.*, arXiv.2204.14140-v1 (2022).

[16] See https://www.luxiumsolutions.com/radiation-detection-scintillators/crystal-scintillators/lanthanum-bromide-labr3 for information about LaBr3 crystals by Luxium.

[17] See https://www.hamamatsu.com/us/en/product/optical-sensors/pmt/pmt-assembly/head-on-type/H10828.html for information about PMT model H10828 by Hamamatsu.

[18] See https://www.caen.it/products/dt5730/ for information about CAEN digitizer model DT5730s.

[19] A. D. Molin, "Reconstruction of the velocity space of runaway electrons by spectral measurements of the hard x-ray emission in tokamaks," Ph.D. dissertation (*Universitá degli Studi di Milano-Bicocca, Department of Physics*, 2021).

[20] M. Nocente, D. Rigamonti, V. Perseo, M. Tardocchi, G. Boltruczyk, A. Broslawski, A. Cremona, G. Croci, A. Gosk, V. Kiptily *et al.*, Rev. Sci. Instrum. **87**, 11E714 (2016).

[21] E. Panontin, D. Rigamonti, M. Nocente, A. Dal Molin, A. Broslawski, T. Craciunescu, G. Croci, N. Cruz, J. Figueiredo, L. Giacomelli *et al.*, Rev. Sci. Instrum. **92**, 053529 (2021).